Nonleptonic weak decay of $^{5}_{\Lambda}$He and $^{12}_{\Lambda}$C

J. J. Szymanski,* P. D. Barnes, G. E. Diebold, R. A. Eisenstein,† G. B. Franklin, R. Grace,‡
D. W. Hertzog,* C. J. Maher, B. P. Quinn, R. Rieder,§ J. Seydoux, and W. R. Wharton**
Physics Department, Carnegie Mellon University, Pittsburgh, Pennsylvania 15213

S. Bart, R. E. Chrien, P. Pile, R. Sutter, and Y. Xu††
Brookhaven National Laboratory, Upton, New York 11973

R. Hackenburg,‡‡ E. V. Hungerford, T. Kishimoto,§§ and L. G. Tang
University of Houston, Houston, Texas 77004

B. Bassalleck
University of New Mexico, Albuquerque, New Mexico 87131

R. L. Stearns
Vassar College, Poughkeepsie, New York 12601
(Received 24 September 1990)

Hypernuclear lifetime and partial decay-rate measurements made at the Brookhaven National Laboratory Alternating Gradient Synchrotron are reported for $^{5}_{\Lambda}$He and $^{12}_{\Lambda}$C. The mesonic and nonmesonic decays are compared to existing weak-interaction calculations. In particular, the nonmesonic reaction $\Lambda N \rightarrow NN$ is discussed as an example of a nonleptonic weak process for which calculations have been reported using various effective weak Hamiltonians.

I. INTRODUCTION

The weak decays of hyperons have been discussed extensively in the literature as examples of nonleptonic weak interactions. The total rates, the partial rates, and the spin-dependent features of the decay modes have been studied. The correct description of these processes requires the development of an effective weak Hamiltonian which takes into account modification of the weak force due to the presence of strongly interacting particles. This paper contains a description of some tests of the effective Hamiltonian in the context of new measurements of the lambda-nucleon weak interaction as extracted from hypernuclear weak decay.

A. Physics motivation

Although the weak decay of the lambda hyperon has been studied for 40 years, the partial mesonic decay rates are not well understood in terms of the underlying weak Hamiltonian. The mesonic decay into a pion and nucleon may be described in terms of the exchange of a W boson between quarks as shown in Fig. 1(a). One expects that a similar mechanism should also describe the weak interaction of a lambda and a nucleon in which two nucleons are produced, as shown in Fig. 1(b).

At zero momentum transfer and in the absence of a strong interaction, the lowest-order weak Hamiltonian for the quark-quark interactions of Fig. 1 is the result of the combination of $V-A$ theory with the Cabibbo hypothesis:[1]

$$H_{V-A}=\frac{G_F}{\sqrt{2}}\sin\theta_C\cos\theta_C Q_{V-A}+\text{c.c}\ , \tag{1}$$

where G_F is the Fermi coupling constant, θ_C is the Cabibbo angle which characterizes the flavor mixing, and the operator Q_{V-A} is

$$Q_{V-A}=\bar{u}\gamma_\mu(1-\gamma_5)s\bar{d}\gamma^\mu(1-\gamma_5)u\ . \tag{2}$$

This Hamiltonian leads to both $\Delta I=\frac{1}{2}$ and $\Delta I=\frac{3}{2}$ transitions with comparable strength. It is well known,[2] however, that both kaon decay and free hyperon decay data suggest that the $\Delta I=\frac{1}{2}$ amplitude is about a factor of 20 stronger than the $\Delta I=\frac{3}{2}$ amplitude. The origin of this empirical "$\Delta I=\frac{1}{2}$ rule" is not understood and the derivation of the complete Hamiltonian, which has the correct isospin character, is a problem widely discussed in the literature.

Strong interaction modifications to the $V-A$ form of the Hamiltonian in the quark-W-boson description of Eq. (1) have been discussed by many authors.[2–5] Gilman and Wise have discussed soft gluon exchange corrections and the addition of explicit $\Delta I=\frac{1}{2}$ diagrams, such as the type shown in Fig. 2, in an attempt to explain the observed enhancement in the $\Delta I=\frac{1}{2}$ strength. However, they find only a factor of 4 enhancement.[3]

An alternative viewpoint for discussing nonmesonic Λ decay is the meson exchange description shown in Fig. 3, in which the meson is exchanged between a weak vertex and a strong vertex. In meson exchange, the $\Delta I=\frac{1}{2}$ rule is put into the weak vertex Hamiltonian explicitly:

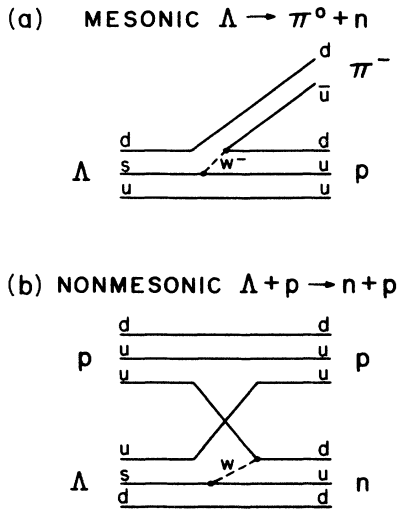

FIG. 1. Examples of quark flow diagrams for (a) mesonic and (b) nonmesonic decays of the Λ hyperon.

$$H_{\pi\ \text{exchange}} = iG_w \Psi_N (1+\lambda\gamma_5)\tau\cdot\Psi_\Lambda \phi_\pi \ , \tag{3}$$

where λ and G_w are empirical constants, Ψ_N and ϕ_π are the nucleon and pion fields, and Ψ_Λ is the Λ spurion field, which is used to enforce the $\Delta I = \frac{1}{2}$ rule.

The nonmesonic transition can be described with meson exchange or with the quark language. The $\Delta I = \frac{1}{2}$ rule is not yet fully understood, but progress has been made using quark models which include strong-interaction corrections to the weak Hamiltonian. As further tests of these calculations, we investigate nonmesonic transition rates obtained from new measurements of hypernuclear decay.

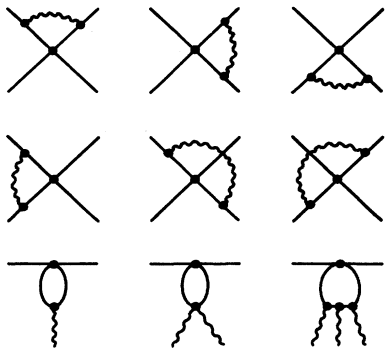

FIG. 2. Strong-interaction corrections to the quark-quark weak interaction considered by Gilman and Wise. The last rows shows the penguin diagrams which contribute only to the $\Delta I = \frac{1}{2}$ transitions.

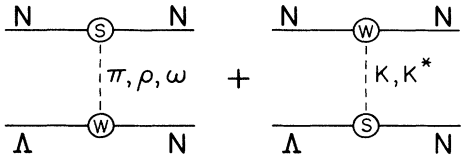

FIG. 3. Meson-exchange description of the nonmesonic decays.

B. Hypernuclear weak decay

In most cases, a particle-stable hypernucleus will decay electromagnetically to its ground state before undergoing a strangeness-changing weak decay to a normal nucleus. The aim of these experimental studies is a better understanding of these nonleptonic weak interactions.

The predominant decay modes are of two types: mesonic and nonmesonic. The mesonic modes are $\Lambda \to p\pi^-$ (partial rate Γ_{π^-}) and $\Lambda \to n\pi^0$ (partial rate Γ_{π^0}) while the nonmesonic modes are $\Lambda p \to np$ (proton stimulated partial rate Γ_p) and $\Lambda n \to nn$ (neutron stimulated partial rate Γ_n). The leptonic and weak radiative decay modes are orders of magnitude smaller and will be neglected in this discussion. The mesonic modes are analogous too free Λ decay, but are modified in hypernuclei because of phase-space changes and Pauli blocking of the final-state nucleons.[5,6] Conversely, the nonmesonic modes become available in hypernuclei, and are the dominant decay modes for all but the smallest hypernuclear systems. An experimental attraction of the nonmesonic modes is the ease of their identification because of the energetic nucleons produced in the final state. The total mesonic decay rate is denoted Γ_m, where $\Gamma_m = \Gamma_{\pi^-} + \Gamma_{\pi^0}$, and the total nonmesonic decay rate is denoted Γ_{nm}, where $\Gamma_{nm} = \Gamma_p + \Gamma_n$. The sum of all four partial rates gives the total decay rate $\Gamma_{\text{total}} = 1/\tau$ for a particular hypernucleus.

C. Experimental situation

Measurements of hypernuclear decay partial rates are still quite sparse. In fact, there is no single hypernucleus for which the complete set of partial rates has been measured. One or more of the following quantities have been measured for a few hypernuclei: the lifetime, the ratio of the neutron and proton stimulated partial rates Γ_n/Γ_p, and the ratio of the nonmesonic and the charged pion partial rates $\Gamma_{nm}/\Gamma_{\pi^-}$. The uncertainties on the measured values are often quite large as can be seen in Tables I and II, which show the existing measurements of Γ_n/Γ_p and $\Gamma_{nm}/\Gamma_{\pi^-}$, respectively. A recent measurement of π^0 branching ratios by Sakaguchi *et al.* gives $\Gamma_{\pi^0}/\Gamma_{\text{total}} = 0.166 \pm 0.055$ for ${}^{12}_{\Lambda}$C decay and an upper limit of $\Gamma_{\pi^0}/\Gamma_{\text{total}} < 0.291$ for ${}^{11}_{\Lambda}$B decay.[8] Table III shows the existing information on hypernuclear lifetimes. Many of the measurements are based on very limited statistics, such as the ${}^{16}_{\Lambda}$O lifetime measurement (22 events).

TABLE I. Existing measurements of the ratio Γ_n/Γ_p. These results were originally quoted as the ratio $n=\Gamma_n/(\Gamma_p+\Gamma_n)$.

Hypernucleus	Γ_n/Γ_p	Reference
$^{4}_{\Lambda}$He	$0.43^{+0.24}_{-0.18}$	9
	$0.67^{+0.19}_{-0.15}$	10
$^{5}_{\Lambda}$He	$0.77\rightarrow 2.0$	11
	≥ 1.4	12
$_{\Lambda}$B, $_{\Lambda}$C, $_{\Lambda}$N	$0.59^{+0.17}_{-0.14}$	13
$A>10$	$2.1^{+0.45}_{-0.27}$	14
$A\sim 40-100$	$1.5\rightarrow 9$	15
	5.7	16
	9	17

The nonmesonic weak decay rates of S- and P-shell hypernuclei, such as the $^{5}_{\Lambda}$He and $^{12}_{\Lambda}$C rates reported in this paper, are of particular interest in the study of the nonleptonic weak interaction $\Lambda+N\rightarrow N+N$, since they provide insight into spin-isospin structure of the Hamiltonian. The seminal works in this interpretation of hypernuclear decays were the investigations of hydrogen and helium hypernuclei by Block and Dalitz[6] in the early 1960s.

This paper describes measurements of $^{5}_{\Lambda}$He and $^{12}_{\Lambda}$C weak decays. The experimental goals were (1) to measure excitation energy spectra with and without decay product tags, (2) to measure hypernuclear lifetimes (the $^{12}_{\Lambda}$C lifetime result has been previously reported in Ref. 7), and (3) to detect protons and neutrons from nonmesonic decay and charged pions from mesonic decay in order to extract the partial decay rates. The apparatus is described in Sec. II. We report the results in Sec. III. Recent calculations of the effective weak Hamiltonian and its application to this problem are reviewed and compared to the new measurements in Sec. IV.

II. APPARATUS

The experimental apparatus changed slightly between the $^{12}_{\Lambda}$C and $^{5}_{\Lambda}$He measurements, which were performed in two separate runs. Such changes will be noted where they affect the performance of the apparatus.

TABLE II. Existing measurements of the ratio $\Gamma_{nm}/\Gamma_{\pi^-}$.

Hypernucleus	$\Gamma_{nm}/\Gamma_{\pi^-}$	Reference
$^{4}_{\Lambda}$He	0.26±0.13	9
$^{4}_{\Lambda}$H	0.52±0.10	9
	0.70±0.19	18
$^{5}_{\Lambda}$H	1.31±0.09	19
	1.2±0.2	11
$^{4,5}_{\Lambda}$He	1.01±0.12	20
$_{\Lambda}$Li	2.55±0.66	20
$_{\Lambda}$Li, $_{\Lambda}$Be	2.4 ±0.7	21
$_{\Lambda}$Be	4.3 ±1.1	13
$\geq{}_{\Lambda}$Be	6.6 ±1.4	20
$^{11}_{\Lambda}$B	4.8 ±1.1	13
$\geq{}_{\Lambda}$B	5.3 ±1.3	20
$_{\Lambda}$B, $_{\Lambda}$C, $_{\Lambda}N$	5.9 ±1.2	19
	5.5 ±0.5	13
$40<A<100$	100–200	15

TABLE III. Existing lifetime measurements.

Hypernucleus	Lifetime (psec)	Reference
$^{3}_{\Lambda}$H	95±20	9
	90^{+220}_{-40}	22
	264^{+84}_{-52}	23
	246^{+62}_{-41}	24
	128^{+35}_{-26}	25
	285^{+127}_{-105}	28
$^{4}_{\Lambda}$H	180^{+250}_{-70}	22
	200±80	26
	268^{+166}_{-107}	28
$^{4}_{\Lambda}$He	≥ 100	27
	228^{+233}_{-129}	28
$^{5}_{\Lambda}$He	140^{+190}_{-50}	22
	180^{+150}_{-60}	27
	251^{+190}_{-73}	28
	274^{+60}_{-50}	29
$^{16}_{\Lambda}$O	86^{+33}_{-26}	30
$_{\Lambda}$U	100^{+100}_{-50}	31
$_{\Lambda}$Bi	250^{+250}_{-100}	32
	2700±500	33

A. Hypernuclear production and tagging

The experiments used the $^{A}Z(K^-,\pi^-)^{A}_{\Lambda}Z$ reaction to produce and tag hypernuclear states. K^- mesons were produced in a platinum target by 28 GeV/c protons from the Brookhaven National Laboratory Alternating Gradient Synchrotron (AGS). A K^- beam was generated with the Low Energy Separated Beam I (LESB I). The end of the beam line consisted of a magnetic spectrometer, shown at the bottom of Fig. 4, which allowed event-by-event evaluation of the incident K^- momentum. The K^- beam had a ±2.5% momentum bite, a π^--to-K^- ratio roughly 10 to 1, and a flux of $\sim 1.2\times 10^5$ K^-/sec. A 4-gm/cm^2 scintillator target was exposed to the 800 MeV/c K^- beam to produce $^{12}_{\Lambda}$C. A 95.6% pure ^{6}Li target was used to produce $^{6}_{\Lambda}$Li, the ground state of which decays via proton emission to $^{5}_{\Lambda}$He. The outgoing π^-'s were then momentum analyzed by a second magnetic spectrometer (Moby Dick), also shown in Fig. 4.

The incident K^-'s were identified in hardware using the 2.77 nsec time-of-flight difference between 800 MeV/c kaons and pions traversing the 5.2-m flight path between the trigger counters $S1$ and ST1 shown in Fig. 4. Additional K-π separation was achieved with the two critical angle Cherenkov detectors CK and $C\pi$, which identified kaons entering the beam magnetic spectrometer and pions leaving the beam magnetic spectrometer, respectively. Identification of the outgoing π^- was accomplished by time of flight between ST1 and the two counters $S2$ and $S3$. The (K^-,π^-) events were distinguished from $K^-\rightarrow\mu^-\bar{\nu}$ decays by their kinematic differences. A muon detector, used for additional separation of π^-'s from μ^-'s, was situated at the end of the hypernuclear spectrometer system, downstream of $S3$, during the $^{6}_{\Lambda}$Li measurement. This detector consisted of a scintillator preceeded by a 43.5-cm-thick steel slab which

absorbed pions via their strong interactions; the slab was not thick enough to stop the 730-MeV/c μ^-'s from the background decay $K^- \rightarrow \mu^- \bar{\nu}$.

Particle trajectories were measured by a set of 18 drift chambers located at the entrances and exists of both magnetic spectrometers.[34] The 576-nsec time window on the drift chambers resulted in a 30% probability of two or more hits in the drift chamber at the entrance to the beam magnetic spectrometer due to high counting rates in this area. A scintillator hodoscope was located just upstream of the first drift chamber to give a short time window coincidence with the correct hit in the first drift chamber. There were redundant chambers included in key locations throughout the system, allowing an overall (K^-,π^-) reconstruction efficiency of approximately 45%.

Reconstruction of the K^- and π^- trajectories through their respective spectrometers allowed the calculation of the invariant mass of the unobserved strange system. Hypernuclear states were seen as peaks in these excitation spectra. We achieved a momentum resolution of $\Delta P/P=0.6\%$ FWHM with the 5.87-gm/cm^2 ^{6}Li target using this method.

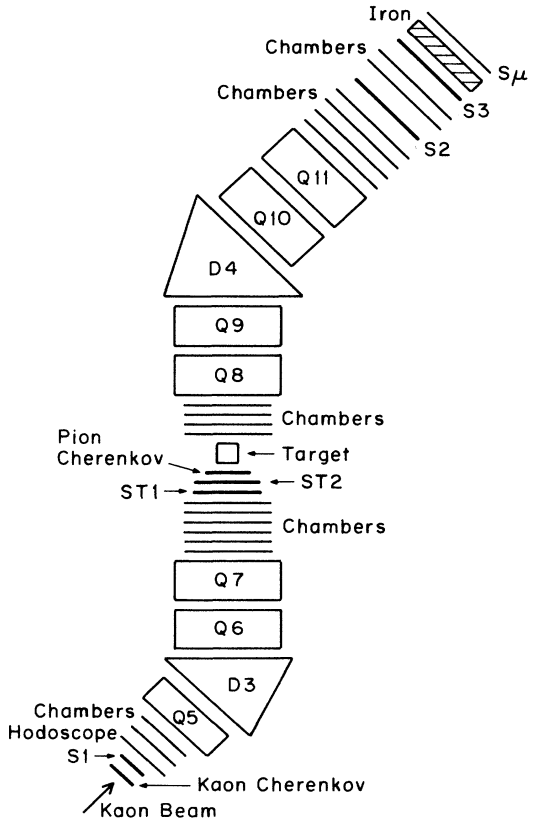

FIG. 4. The Low Energy Separated Beam at the Brookhaven AGS and the hypernuclear spectrometer (Moby Dick). Elements $D3$ and $D4$ are the dipoles of LESB I and Moby Dick spectrometer, respectively. The quadrupoles are labeled $Q5$–$Q11$; $S1$, $ST1$, $ST2$, $S2$, and $S3$ are timing scintillators. $S\mu$ is the muon tag scintillator.

B. Detection of decay products

The target was surrounded by two detector systems designed to detect hypernuclear decay products (see Fig. 5). Above the target was a neutron counter array which measured neutron energies by time of flight. Below the target sat a π^-/p spectrometer to detect charged decay products. The π^-/p spectrometer used range, energy, and dE/dx information to identify π^-'s and p's. It also provided time and trajectory information.

The neutron counter consisted of an array of plastic-scintillator bars with a layer of thin veto counters mounted along the lower and upstream edges to detect charged particles which entered the neutron counter array. Particles which deposited energy in the thick neutron counters within a 100-nsec gate around the in-beam (K^-,π^-) trigger, but which did not fire the thin veto counters, were considered neutrons. Each neutron detector element was $183\times15\times5$ cm^3 bar of PILOT F scintillator connected on each end via a tapered light guide to an XP2230 photomultiplier tube. The veto detectors were each 1.0-cm thick and together covered the entire entrance face of the array.

The efficiency of the array depended both on neutron energy and on a threshold cut on the pulse heights. The neutron counter efficiency was calculated[35] by Monte Carlo methods and the threshold cuts were calibrated by using the known average energy loss of cosmic rays. For the 30–130-MeV neutron kinetic-energy range used in this work, the average efficiency of the three-layer-thick array was calculated to be 0.13 for 10-MeVee (MeV electron equivalent) and 0.16 for 5-MeVee thresholds. The time-of-flight resolution of these detectors for pulse heights typical of neutron interaction was measured to be 0.25-nsec FWHM with the laser monitoring system de-

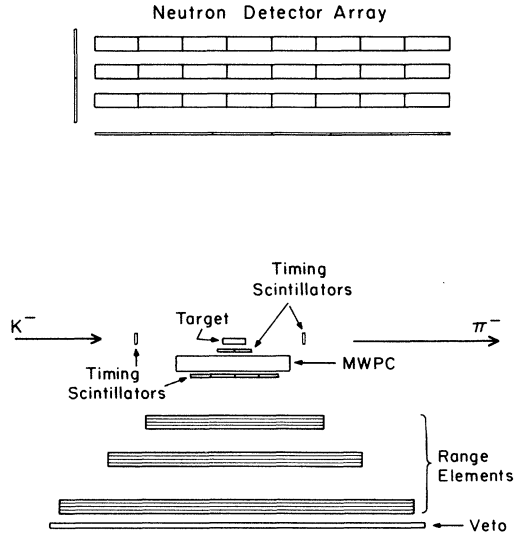

FIG. 5. Pion-proton range spectrometer and neutron detector used to detect hypernuclear decay products shown as setup for $^{12}_{\Lambda}$C measurements.

scribed in Sec. II C. For the $^{12}_{\Lambda}$C measurement, the array consisted of three rows of eight counters mounted 150 cm above the target while the $^{6}_{\Lambda}$Li experiment, used three rows of six counters 90 cm above the target, giving solid angles for the arrays of 0.60 or 0.95 sr, respectively. With the array in position 90 cm above the target, the energy resolution varied from 15.5 to 19.4% for neutrons of energy 30–150 MeV.

The first two scintillator layers of the π^-/p spectrometer were high-quality timing scintillators which gave the decay time of the hypernucleus (see the following discussion of fast-timing techniques). They were constructed of PILOT U scintillator and RCA 8575 photomultiplier tubes. The next 12 scintillator layers were 0.63-cm-thick slabs of NE102 arranged in three packets of four scintillators each; see Fig. 5. The total light output of the charged particles traveling through the range telescope was read out with 26 PM2412 phototubes. The stopping layer was obtained from XP2230 phototubes which read out the individual layers within each packet via BBQ wave-shifter strips positioned along one edge of each layer. A multiwire proportional chamber (MWPC) containing two sets of orthogonal planes gave particle trajectory information. The MWPC measured the quantity $\cos(\theta)$ with an average of better than 0.01 FWHM, where θ is the angle between the particle's trajectory and the axis of the range spectrometer. The last element in the range spectrometer was a scintillator used to veto the charged particles which passed through the entire range spectrometer.

The π^-/p spectrometer had an energy resolution of $\sim$15% and a time resolution of $\sim$200-psec FWHM. Its solid angle was 1.76 sr for the $4\times12\times1$ cm^3 $^{12}_{\Lambda}$C (scintillator) target and 1.25 sr for the $11\times11\times3$ cm^3 $^{6}_{\Lambda}$Li target. The difference in solid angles between the two experiments arose because the targets were different sizes. The range spectrometer was calibrated using the known energy deposition of minimum ionizing pions which passed through the entire stack and of protons which stopped through the stack. Charged particles which entered the π^-/p spectrometer were identified by comparing the number of slabs traversed (range) with the energy deposited in the last completely traversed layer, ΔE_{meas}. The range information was used to give ΔE_{calc} for the particle under the hypothesis that it was a proton and the quantity $\text{PID}=\Delta E_{\text{calc}}-\Delta E_{\text{meas}}$ clearly distinquishes protons from pions as shown in Fig. 6. For additional π^-/p particle separation, the total energy of the particle E_{meas} was derived from the total light collected from all but the stopping layer and compared to the energy E_{calc}, expected based on the range information. The light from the stopping layer was ignored to reduce the influence of additional light from stopped π^- nuclear absorption.

C. Fast-timing measurements

The measurement of the hypernuclear lifetimes required accurate timing. The lifetime was measured directly, using two timing scintillators in the kaon beam to measure the production time of the hypernucleus and using the two timing scintillators in the range spectrometer to measure the decay time of the hypernucleus. The two in-beam timing scintillators *ST*1 and *ST*2 measured $15\times4\times1.3$ cm^3 and $15\times4\times1.6$ cm^3 and used XP2020 photomultiplier tubes. There are several effects which limit the timing resolution of scintillation counters, including time walk due to pulse-height differences, errors in time corrections applied to account for the time of flight between the timing scintillators and the target, long-term time drift, and the intrinsic resolution of the detectors. The time walk was minimized by using Phillips Electronics 715 constant-fraction discriminators to discriminate the photomultiplier pulses. Errors in the time-of-flight corrections were minimized by placing the timing scintillators as close as possible to the target.

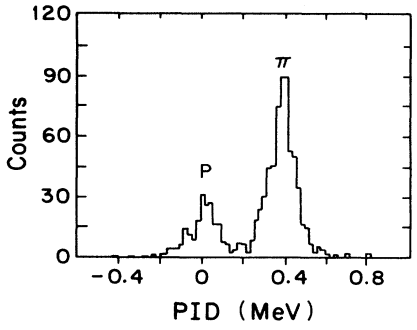

FIG. 6 Particle identification plot showing proton and pion peaks. The horizontal axis is the difference between the measured energy loss in the π^-/p spectrometer and that calculated based on the observed range, assuming the particle is a proton.

The intrinsic resolutions of the scintillation detectors were limited by statistical effects in the propagation time of photons in the scintillator material and electrons in the photomultiplier tubes. The intrinsic resolution was optimized by maximizing the amount of light which was produced in the scintillator and transported to the photomultiplier tubes. All of the timing scintillators were designed so that the cross-sectional area of the scintillators matched the active area of the photomultiplier tubes, and so that no twisted light guides were necessary. The spectrometer counter scintillators were glued directly onto the XP2020 phototubes and two timing scintillators in the range spectrometer were each segmented into pieces with cross section 4.0×0.63 cm^2 or 4.5×0.63 cm^2.

Timing resolution and long-term time drifts were measured with a laser time-monitor system. A nitrogen laser emitted a 200-psec long pulse of ultraviolet light (wavelength=337.1 nm) which was attenuated by neutral density filters to prevent photomultiplier tubes from saturating. A quartz optical flat split the beam into two parts, one of which was attenuated and directed into a photomultiplier tube to provide a scintillator-independent time-walk monitor. The remainder of the beam was further attenuated by a rotating variable-attenuator filter wheel, which rotated between pulses to vary the amplitude of the laser light pulse sent to the scintillators by a factor of 10. The light-pulse amplitude was varied so that the time response of the timing scintillators could be

mapped out as a function of pulse height. Each light pulse was split and guided to each of the scintillators through a system of fused-silica optical fibers. The ultraviolet light excited the scintillation material which, in turn, produced a pulse of visible light closely resembling a light pulse produced by a charged particle.

The laser time-monitor system allowed us to measure the time drifts which occurred over the several weeks of data collection. Over the 2 week ${}^{5}_{\Lambda}$He run, for example, the zero time varied by ± 100 psec without the time-drift correction, and varied by ± 20 psec after the time-drift correction. The lifetime measurements and measured timing resolution are discussed in Sec. III B.

III. ANALYSIS AND RESULTS

A. Hypernuclear spectroscopy results

The hypernuclear mass spectrum for the ^{6}Li target is shown in Fig. 7(a). The mass spectra obtained in coincidence with a decay proton ($E_p > 30$ MeV) or a pion ($E_\pi > 15$ MeV) detected in the π^+/p spectrometer are shown in Figs. 7(b) and 7(c), respectively. The solid curves are the results of fits which are discussed in the following sections. The ground state is clearly seen in the proton-coincident spectrum, Fig. 7(b), while it only appears as a shoulder in the pion-coincident spectrum, Fig. 7(c). Some of the coincident π^- mesons which correlate to the events in the high-excitation region of Fig. 7(c) are believed to originate from a background of free-lambda decays. These free lambdas may be produced through quasifree production or through the emission of lambdas from particle unstable resonances. The proton-coincident spectra are not contaminated by these events since the free-lambda decays do not produce protons with energies above the 30-MeV threshold.

We identify the two peaks at 0- and 17-MeV excitation energy in Fig. 7(b) as the ground state $n(p_{3/2}^{-1})\Lambda(s_{1/2})$ of ${}^{6}_{\Lambda}$Li and the S-substitutional state $n(s_{1/2}^{-1})\Lambda(s_{1/2})$. Figure 7(b) can be compared to the earlier measurements of Bertini *et al.*[36] shown in Fig. 8. The latter data were also obtained with the (K^-,π^-) reaction but at a momentum transfer of 50 MeV/c compared to the value of ~ 140 MeV/c in the current work. The lower momentum transfer only weakly excites the ground state and strongly excites the S-substitutional state at an excitation energy of 18 MeV. In addition, the Bertini measurement reveals a third peak at 8 MeV which they identify as the P-substitutional state $n(p_{3/2}^{-1})\Lambda(p_{1/2})$. This state is not seen in the present proton-coincidence measurement spectrum, Fig. 7(b). This suggests that the state decays through Λ emission. The resulting free lambda cannot participate in nonmesonic weak decay and thus the energetic proton required for the proton-coincident excitation energy spectrum is not produced. This is consistent with the interpretation presented by Bertini *et al.*,[36] Majling *et al.*,[37] and Auerbach and Giai[38] in which the large width ($\Gamma = 7-10$ MeV) of the 8-MeV state is related to its particle-unstable character. There is evidence of the P-substitutional state at 8.5 MeV in the pion-coincident excitation energy spectrum, Fig. 7(c) further confirming the interpretation that this state breaks up by Λ emission.

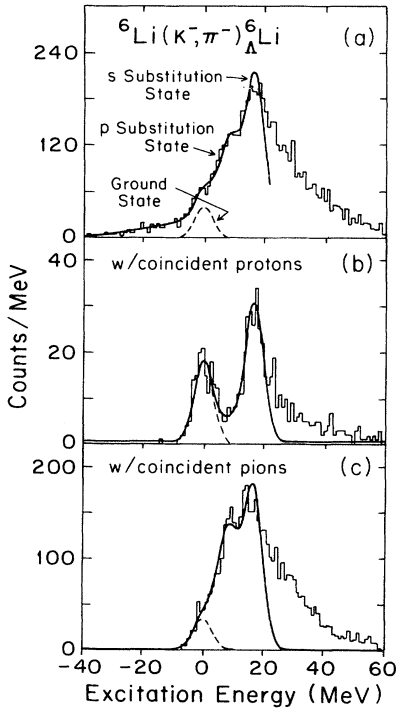

FIG. 7. Comparison of hypernuclear excitation spectra for ${}^{6}_{\Lambda}$Li. (a) No coincidence, (b) in coincidence with decay protons $E > 30$ MeV, and (c) in coincidence with decay pions $E > 15$ MeV. The solid line shows the total fit and the dashed line shows contribution of ground state alone.

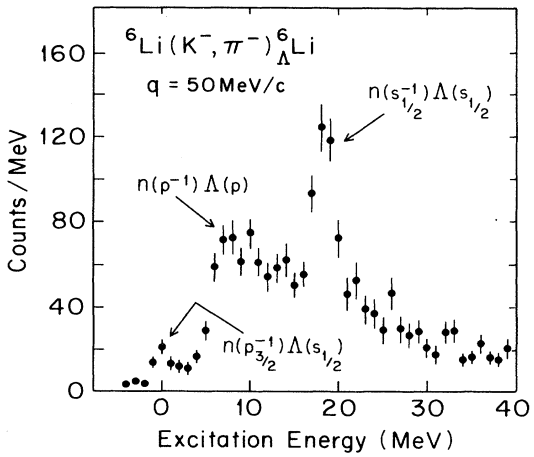

FIG. 8. Hypernuclear states observed in ${}^{6}_{\Lambda}$Li by Bertini *et al.* (Ref. 36) in a (K,π) reaction (50-MeV/c momentum transfer) with no detection of decay particles.

We note again that the decay rate measured for events in the low-excitation region of $^{6}_{\Lambda}$Li give the weak decay rates of $^{5}_{\Lambda}$He because $^{6}_{\Lambda}$Li ground state decays to $^{5}_{\Lambda}$He by emission of a proton of 1-MeV kinetic energy.

The hypernuclear mass spectra for the ^{12}C target are shown in Fig. 9. The $^{12}_{\Lambda}$C mass spectrum constructed without a coincident charged-particle requirement, shown in Fig. 9(a), contains a large background from $K^{-}\rightarrow\mu^{-}\bar{\nu}$ events in the ground-state region. The kinematics of this background reaction was not as cleanly separated from the hypernuclear production kinematics as it was for the $^{6}_{\Lambda}$Li case. Therefore, this background is larger in the ^{12}C data than the corresponding $^{6}_{\Lambda}$Li data shown in Fig. 7(a). The $^{12}_{\Lambda}$C measurement was also performed without the benefit of a muon detector at the end of the spectrometer. This background is greatly reduced when the mass spectra are constructed with the requirement of a coincident a decay proton ($E_p > 30$ MeV) or a decay pion ($E_\pi > 15$ MeV), as shown in Figs. 9(b) and 9(c). Figure 9(b) shows three identifiable states while Fig. 9(c) shows very little evidence of the ground state and is mostly a broad structure identified with quasifree Λ production. The decay rates measured for events in the low-excitation region are the weak decay rates of $^{12}_{\Lambda}$C since the ground state is particle stable. The P-substitutional state is known[39] to decay to $^{11}_{\Lambda}$B+p, whereas the breakup of the S-substitutional state is predicted[40] to decay to $^{9}_{\Lambda}$Be.

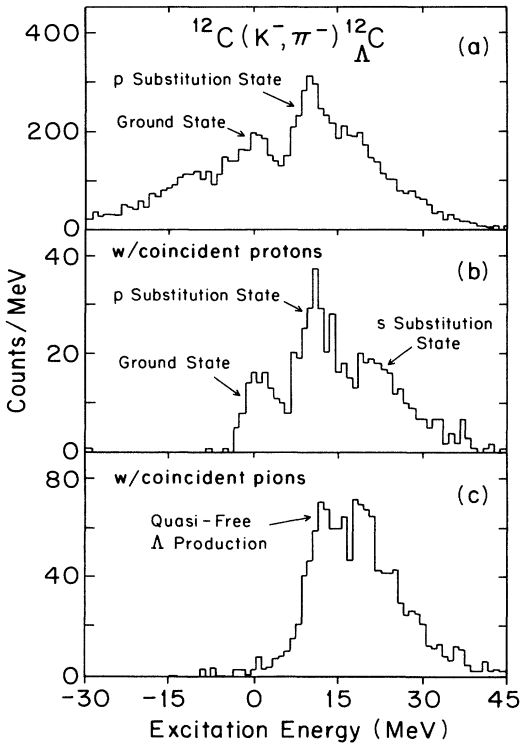

FIG. 9. Comparison of hypernuclear excitation spectra for $^{12}_{\Lambda}$C (a) no coincidence, (b) in coincidence with decay protons, and (c) in coincidence with decay pions.

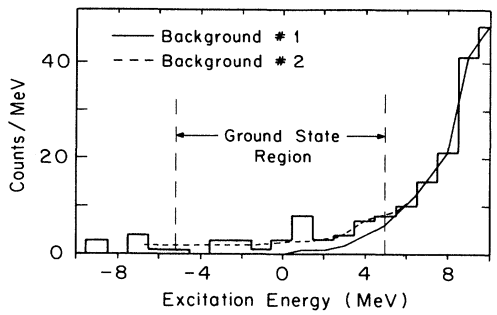

FIG. 10. $^{12}_{\Lambda}$C excitation energy spectrum in the ground-state region with pion coincidence including two possible estimates of background shapes.

B. Charged-particle decay modes of $^{6}_{\Lambda}$Li, $^{5}_{\Lambda}$He, and $^{12}_{\Lambda}$C

Peak in the $^{6}_{\Lambda}$Li excitation energy spectra, obtained in coincidence with protons or pions in the range spectrometer, were fitted in order to extract the number of events which produced decay protons or pions for each hypernuclear state. Figure 7(b) shows the fit to the coincident proton excitation energy spectrum. The fitting function was a sum of three Gaussians, representing the three hypernuclear states, plus a flat background. Since the P-substitutional state is not clearly seen in this spectrum, the separation between the ground state and the P substitutional was set to 8.5 MeV (as determined from the Bertini data) and the rms width of the state was set to 3.5 MeV to be consistent with the experimental resolution of this work. The results of this fit were the width and position of the ground state and S-substitutional state along with the total counts in each of the three states, as listed in Table IV. The spectrum was fitted only up to an excitation energy of 20 MeV; states at higher-excitation energy were not resolved in this experiment. The rms widths and centroids found for the ground state and S-

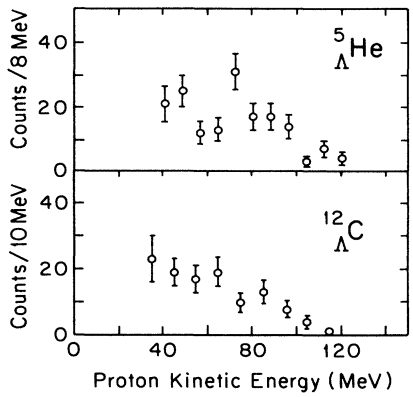

FIG. 11. Proton energy spectra for $^{5}_{\Lambda}$He (top) and $^{12}_{\Lambda}$C (bottom) nonmesonic decay.

TABLE IV. The number of coincident events. The $^{6}_{\Lambda}$Li results were extracted by fits to $^{6}_{\Lambda}$Li excitation spectra. The $^{12}_{\Lambda}$C results were obtained from the number of counts between cuts in the $^{12}_{\Lambda}$C excitation spectra.

$^{6}_{\Lambda}$Li data	Ground state	Proton coincidence $p^{-1}p$ state	$s^{-1}s$ state	Pion coincidence Ground state
Centroid	−0.1±0.5	8.5 MeV (input)	16.8±0.4 MeV	0.1 MeV (input)
Width	3.1±0.5 MeV	3.5 MeV (input)	3.1±0.4 MeV	3.1 MeV (input)
Detected decays	136±20	40±16	233±23	258 ±47
Total decays	1730±260			3180±580
$^{12}_{\Lambda}$C data	Ground state	Proton coincidence		Pion coincidence Ground state
Detected decays	114±16			<37
Total decays	1410±200			<450

substitutional state from this fit to the coincident proton excitation data were used in the fit to the pion-coincident $^{6}_{\Lambda}$Li excitation energy spectrum shown in Fig. 7(c). The position and width of the *P*-substitutional state were again taken to be 8.5 and 3.5 MeV.

The $^{12}_{\Lambda}$C excitation spectra for events with coincident protons and pions, shown in Figs. 9(b) and 9(c), were analyzed without fitting peaks to the states. Instead, the number of counts in the region from −5 to +5 MeV was used to extract the number of events from the ground state. In contrast to the proton-coincident excitation spectrum, the ground state is only seen as a small enhancement in Fig. 9(c) and a significant portion of the counts in this region may be background not associated with the ground state. Two models of the background, shown in Fig. 10, were used to determine the number of pions from the ground state. Subtraction of a Gaussian background, fit to the quasifree peak, leaves 25 pions from the decay of the ground state while a subtraction of a fit of a Gaussian plus an additional flat background leaves 5 pions, which is statistically insignificant. At the 95% confidence level, the data give an upper limit of 37 for the detected number of π^- mesons from the ground state of $^{12}_{\Lambda}$C.

Figure 11 shows the proton energy spectra, after energy acceptance corrections, corresponding to the ground-state excitation regions of the two experiments. The $^{5}_{\Lambda}$He proton energy distribution shows some evidence of the peak expected near 75 MeV but there is no sign of a peak in the $^{12}_{\Lambda}$C distribution. This can be understood as arising from the larger probability for final-state interactions of the outgoing protons in $^{12}_{\Lambda}$C (see Sec. III E for a discussion of the final-state interaction effects in these experiments).

The raw number of hypernuclear decays to protons or pions must be corrected for acceptance and efficiency in order to extract partial decay rates. The acceptance of the π^-/p spectrometer as a function of energy is calculated with a Monte Carlo program and the resulting product of efficiency and solid angles are $\Delta\Omega_{\text{eff}}=1.59$ sr for the $^{12}_{\Lambda}$C experiment and $\Delta\Omega_{\text{eff}}=1.11$ sr for the $^{5}_{\Lambda}$He experiment. The tracking efficiency of the MWPC in the π^-/p spectrometer was 64% for the $^{12}_{\Lambda}$C experiment and 89% for the $^{5}_{\Lambda}$He experiment; the difference in efficiency arises because much stricter criteria was applied in the analysis of the $^{12}_{\Lambda}$C experiment. The total number of events which decayed by emission of energetic protons (>40-MeV kinetic energy), after acceptance corrections, are given in Table IV.

C. Detection of neutrons from hypernuclear decay

To determine the number of decay neutrons from $^{5}_{\Lambda}$He and $^{12}_{\Lambda}$C events using the neutron detector array data, corrections for the energy-dependent efficiency, accidental background, and coincident neutron background from π^--capture stars had to be performed. This section discusses these corrections. The final results for the neutron-stimulated partial rates are given in Sec. III E.

Figure 12 shows the β^{-1} (c/velocity) spectrum for neutral events above a 10-MeVee threshold in the neutron counter array with excitation energy in the ground-state region of $^{12}_{\Lambda}$C. The events with $\beta^{-1}>10$ give a measurement of the random time background, since true coincidence neutrons in this region would have kinetic energies less than the detector threshold. The flat time back-

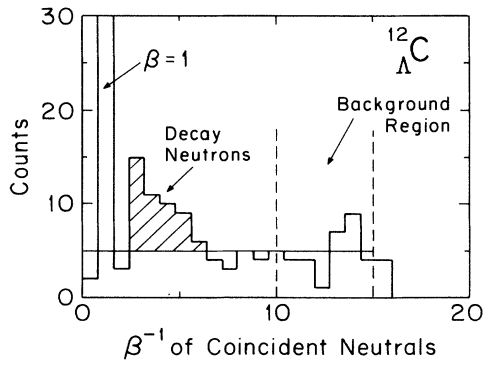

FIG. 12. β^{-1} spectrum for neutral events from the $^{12}_{\Lambda}$C ground-state region. The neutron detectors have a 10-MeVee threshold applied for this spectrum.

ground determined in this way was subtracted from the total number of counts in the region with $\beta^{-1} < 10$, which contains neutral events with kinetic energies above threshold. The number of counts in excess of background was determined as a function of neutron kinetic energy and an efficiency correction was applied.

For the $^{12}_{\Lambda}$C ground-state region, the number of neutral counts in the neutron counters after subtraction of the random-time background was 40.9 and 17.8 counts for threshold of 5 and 10 MeVee, respectively. After making the efficiency corrections, the number of neutrons with kinetic energy $T_n > 30$ MeV which passed through the neutron detector was found to be 165±54. Taking the solid angle of the neutron detector into account and assuming isotropic distributions gives the total number of neutrons with $T_n > 30$ MeV, $N_n = 3400 \pm 1100$. The corresponding number for the *P*-substitutional state region is $N_n = 4800 \pm 1200$. These numbers include the neutrons which were created when π's from either free- or bound-lambda-decay stopped and annihilated in the materials surrounding the hypernuclear production target. These neutrons cannot be distinguished from hypernuclear decay neutrons. In the $^{12}_{\Lambda}$C experiment, however, the measured π^- branching ratio is quite low and the π^- annihilation background does not make significant background in the $^{12}_{\Lambda}$C neutron measurement.

For $^{5}_{\Lambda}$He decay events (events for which the excitation energy is in the region of the $^{6}_{\Lambda}$Li ground state), the number of neutral counts in the neutron counters after subtraction of the random-time background is 18.7 and 9.5 counts for thresholds of 5 and 10 MeVee, respectively. Since the π^- branching fraction was expected to be higher for the $^{5}_{\Lambda}$He measurement than for the $^{12}_{\Lambda}$C measurement, background neutrons from π^- capture were a potential problem. To reduce this potential background, the ^{6}Li target was surrounded by an array of scintillation counters which served as a charged-particle veto and only events in which none of these veto counters fired were used in the neutron partial rate analysis. Although 87% of the solid angle as seen by the target was covered by this veto, there were still enough π^-'s produced that an estimated 19% of the neutron signal seen in the $^{5}_{\Lambda}$He experiment may be due to π^- annihilation background. This correction was calculated by combining the measured π^- rate with the results of a Monte Carlo of the target geometry. It was found that, of the 9.5±3.0 neutron counts left after the random background subtraction at the 10-MeVee threshold, 1.8±1.4 of these were due to neutrons from π's which either stopped in the target or escaped the target veto and stopped in the surrounding material. The number of neutrons used in the neutron partial rate analysis was then 7.7±3.3. This number is used, along with correction factors from cuts in the ground-state $^{6}_{\Lambda}$Li excitation spectrum, the neutron detector solid angle and detector efficiencies, to give total number of neutrons emitted from the $^{5}_{\Lambda}$He decays in which no charged particle left the target, $N_n = 3000 \pm 1300$.

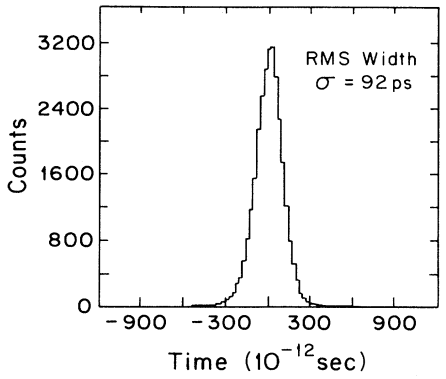

FIG. 13. Time response function measured with the timing scintillators using the prompt reaction: ^{6}Li(π^-,p)X. This spectrum was accumulated during the entire 2-week run.

D. Lifetime measurements

The production and decay times of hypernuclei are measured directly by two timing scintillators in the K^- beam and two timing scintillators in the range spectrometer of Fig. 5. The shape and centroid of the time-resolution function are monitored continuously throughout the experiment with the "prompt" ^{6}Li(π^-,p)X and ^{12}C(π^-,p)X reactions utilizing the pion component of the beam. The resolution function for the entire 2 week $^{5}_{\Lambda}$He run is plotted in Fig. 13 and has a rms width $\sigma = 92$ psec. This shape is compared with the proton time-of-flight spectrum from $^{5}_{\Lambda}$He decays in Fig. 14(a). The resolution function has been scaled to match the area of the decay spectrum which clearly shows the time shift due to the lifetime of $^{5}_{\Lambda}$He. The lifetime spectrum is fitted to the convolution of the resolution function with an exponential decay using a fitting algorithm based on poisson, rather than Gaussian, statistics. The fit extracts a lifetime of 256±21 psec with an effective χ^2 per degree of freedom of 0.86. An identical analysis is performed for $^{12}_{\Lambda}$C, the resulting fit, shown in Fig. 14(b), gives a lifetime of 211±31 psec.[7] In terms of a total decay rate $\Gamma_{\rm tot} = 1/\tau$, the results are

$$\Gamma_{\rm total}(^{5}_{\Lambda}\mathrm{He})/\Gamma_{\Lambda} = 1.03 \pm 0.08 \quad \text{(ground-state region)},$$

$$\Gamma_{\rm total}(^{12}_{\Lambda}\mathrm{C})/\Gamma_{\Lambda} = 1.25 \pm 0.18 \quad \text{(ground-state region)},$$

$$\Gamma_{\rm total}(^{11}_{\Lambda}\mathrm{B})/\Gamma_{\Lambda} = 1.37 \pm 0.16 \quad (^{12}_{\Lambda}\mathrm{C}\ P\text{-substitutional-state region}),$$

$$\Gamma_{\rm total}(^{A}_{\Lambda}\mathrm{Z})/\Gamma_{\Lambda} = 1.31 \pm 0.20 \quad (^{12}_{\Lambda}\mathrm{C}\ S\text{-substitutional-state region}),$$

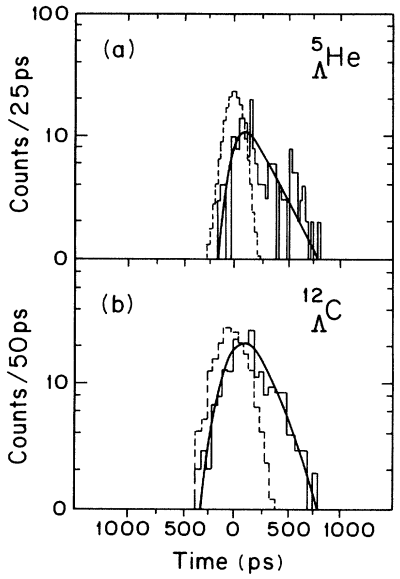

FIG. 14. (a) Time spectrum for $^{5}_{\Lambda}$He proton decay (solid histogram) compared to the normalized time-resolution function of Fig. 13 (dashed histogram). The solid curve shows the fit to the proton time spectrum. (b) Same data for the $^{12}_{\Lambda}$C decays.

where Γ_Λ is the decay rate of a free-lambda particle, $\Gamma_\Lambda = 3.80\times10^{9}$/sec ($\tau_\Lambda = 263$ psec). The errors correspond to one standard deviation.

The lifetime was also measured for regions higher up in the $^{6}_{\Lambda}$Li excitation energy spectrum. The lifetime drops at higher-excitation energy, decreasing from 256±20 psec for the ground-state region down to 160±20 psec in the region around excitation energies of 30 MeV. We attribute the shorter lifetimes at higher-excitation energy regions to the breakup of $^{6}_{\Lambda}$Li into a lighter hypernucleus prior to the weak decay. The lifetime of these species may be shorter than the $^{5}_{\Lambda}$He lifetime because all of the mass 3 and 4 hypernuclei have an open S shell which can contain a final-state nucleon from mesonic decay. This effect is enhanced due to increased phase space. If this additional phase space increases the mesonic rate faster than the nonmesonic rate is decreased due to reduced nucleon density, one would expect shorter lifetimes for the lighter nuclei. Measurements of hypernuclear lifetimes shorter than the 256-psec $^{5}_{\Lambda}$He lifetime have been reported, as listed in Table III.

E. Partial decay rates

The partial decay rates for $^{5}_{\Lambda}$He are calculated from the total number of decays of each type, divided by the total number of hypernuclei produced, multiplied by the total decay rate derived from the lifetime measurements. The number of $^{5}_{\Lambda}$He hypernuclei produced is determined from a fit to the $^{6}_{\Lambda}$Li ground-state region in the excitation energy spectrum with no decay coincidence, as shown in Fig. 7(a). The background to the left and underneath the $^{6}_{\Lambda}$Li ground state in Fig 7(a) is due to $K^- \rightarrow \mu^- + \bar{\nu}$ decays where the inefficiency of the muon veto allows a small portion of the K decays through. Thus, the background shape underneath the ground state is determined from the known shape of the excitation energy spectrum for events in which the muon detector fired. The extracted number of $^{5}_{\Lambda}$He hypernuclei produced is 7400±1200.

Using the quantities derived in the previous sections, the results shown in Table V are obtained for the weak decay rates of $^{5}_{\Lambda}$He. The first column shows the results obtained directly from the measurements of the lifetime, the neutron branching ratio, the proton branching ratio, and the π^- branching ratio. In this case the π^0 rate is obtained by subtracting the other three partial rates from the total rate. Since this calculation of Γ_n has uncertainties due to background corrections and a large uncertainty in Γ_{π^0} due to the propagation of errors in the other measurements, we have also analyzed the data without using the measured number of neutrons by invoking the assumption that $\Gamma_{\pi^0}/\Gamma_{\pi^-} = 0.5$. This assumption is justified if Coulomb effects can be neglected and if the $\Delta I = \frac{1}{2}$ rule is assumed since the states available to the π^- decay mode are isobaric analogs of the states available to the π^0 decay mode. The neutron stimulated rate can then be obtained from

$$\Gamma_n = \Gamma_{\text{total}} - (\Gamma_p + 1.5\Gamma_{\pi^-}) .$$

TABLE V. $^{5}_{\Lambda}$He experimental results.

	Data only	$\frac{\Gamma_{\pi^0}}{\Gamma_{\pi^-}} = 0.5$	With FSI corrections	Previous experiments
$\Gamma_{\text{total}}/\Gamma_\Lambda$	1.03±0.08	same	1.03±0.08	$0.53^{+0.72}_{-0.19}$, Ref. 22, $0.68^{+0.57}_{-0.23}$ Ref. 27) $0.95^{+0.72}_{-0.28}$ Ref. 28, $1.04^{+0.23}_{-0.19}$ Ref. 29
$\Gamma_{\pi^-}/\Gamma_\Lambda$	0.44±0.11	same	0.44±0.11	none
$\Gamma_{\pi^0}/\Gamma_\Lambda$	0.14±0.19	0.22±0.06	0.18±0.20	none
Γ_p/Γ_Λ	0.24±0.06	same	0.21±0.07	none
Γ_n/Γ_Λ	0.21±0.09	0.13±0.20	0.20±0.11	none
$\Gamma_{\text{nm}}/\Gamma_\Lambda$	0.45±0.12	0.37±0.19	0.41±0.14	none
Γ_p/Γ_{π^-}	0.54±0.13	same	0.48±0.15	none
Γ_n/Γ_p	0.87±0.37	0.53±0.83	0.93±0.55	0.077→2.0, Ref. 11, ≥1.4, Ref. 12
$\Gamma_{\text{nm}}/\Gamma_{\pi^-}$	1.02±0.28	0.83±0.22	0.92±0.31	1.2±0.2 Ref. 11, 1.31±0.09, Ref. 20

The results, which are consistent with the calculation of Γ_n using the number of detected neutrons, are shown in the second column of Table V.

The $^{5}_{\Lambda}$He weak-decay widths extracted from the data must also be corrected for final-state interactions of the outgoing nucleus from nonmesonic decay with the spectator nucleons. This was done using an intranuclear cascade model to calculate the modification to the number of detected neutrons and protons due to final-state interactions. A simple model, where the nucleus is a uniform spherical matter distribution of radius 2.1 fm and the mean free path for an outgoing nucleon from nonmesonic decay (energy 10–140 MeV) is 3 fm, was used to estimate the final-state interaction probability to be 0.3 ± 0.1. The final-state interaction corrections change the results by 17% or less and are somewhat insensitive to the large uncertainty we have assigned to the final-state interaction probability. The final $^{5}_{\Lambda}$He weak decay results are listed on the third column of Table V. This analysis was done using the measured neutron branching ratio and does not assume the $\Delta I=\frac{1}{2}$ rule. Only the final-state interaction corrected results will be used in the discussion, since they represent the most sophisticated analysis of these data.

The total number of $^{12}_{\Lambda}$C ground-state events, unbiased by coincidence requirements, would have been needed to extract individual partial rates. However, this number could not be extracted from the data due to uncertainties in the contribution of background reactions in the unbiased sample. Therefore, the individual partial rates for $^{12}_{\Lambda}$C were not produced but rather Γ_{total} and the two ratios Γ_n/Γ_p and $\Gamma_{\pi^-}/\Gamma_{\text{nm}}$, presented in Table VI. The results listed for Γ_n/Γ_p have been corrected for nuclear multiple scattering and charge exchange with an intranuclear cascade calculation[41] (the correction increases Γ_n/Γ_p by $<20\%$). The errors in the total width and the fraction Γ_n/Γ_p are dominanted by statistics. Using the average of the numbers obtained from two background shapes in Fig. 10 to determine the number of decay π^-'s, gives $\Gamma_{\text{nm}}/\Gamma_{\pi^-}=22^{+43}_{-12}$.

In this case, the estimated one-standard-deviation errors are mainly due to uncertainty in the background subtraction. The results can be expressed more clearly as an upper limit on the inverted ratio, $\Gamma_{\pi^-}/\Gamma_{\text{nm}}<0.14$ at the 95% confidence level. This result was obtained by assuming a minimal contribution of decay π^-'s to the ground-state region from higher-excitation energy events. Uncertainties in the fraction of π^- decays which result in neutron coincidences are not significant for the $^{12}_{\Lambda}$C measurements since, unlike the $^{5}_{\Lambda}$He measurements, the number of π^- decays is much smaller than the number of neutron-stimulated decays.

Since fewer partial rates were measured for the $^{12}_{\Lambda}$C decays than for the $^{5}_{\Lambda}$He data, the quantity $\Gamma_{\text{nm}}=(1.14\pm0.20)\Gamma_{\Lambda}$ was extracted using the value $\Gamma_{\pi^0}/\Gamma_{\pi^-}=1.17$. This value was calculated by Gal[42] and is in agreement with more recent calculations by Bando *et al.*[43] The Γ_{nm} result is insensitive to the ratio $\Gamma_{\pi^0}/\Gamma_{\pi^-}$ since the total decay rate is dominated by the nonmesonic rate. The error on the extracted Γ_{nm} was computed using a mesonic rate ratio with an assigned error bar of ±1 ($\Gamma_{\pi^0}/\Gamma_{\pi^-}=1.17\pm1$).

IV. DISCUSSION

A. Comparisons to previous experimental results

The $^{5}_{\Lambda}$He results are compared with earlier measurements in Table V. The present $\Gamma_{\text{total}}/\Gamma_{\Lambda}$ result is consistent with the previous measurements, but with smaller error bars. The most significant partial rate measurements for the present experiment are the Γ_n and Γ_p measurements, which have not been reported before. The values for the Γ_n/Γ_p ratio and the $\Gamma_{\text{nm}}/\Gamma_{\pi^-}$ ratio are consistent with the older experiments but significantly improve the world-averaged rates.

The only other lifetime measurement in the same mass range as $^{12}_{\Lambda}$C is the $^{16}_{\Lambda}$O lifetime measurement of Nield *et al.*[30] The $^{16}_{\Lambda}$O measurement used an ^{16}O beam and a polyethyelene target; K^+ emission was used as the hypernuclear production trigger. A large background was observed in the experiment due to interactions with drift chamber windows. After these background events were identified and subtracted, a total of 22 events were left. The extracted lifetime from the recoil distance distribution was $\tau=86^{+33}_{-26}$ psec or $\Gamma_{\text{total}}(^{16}_{\Lambda}\text{O})/\Gamma_{\Lambda}=3.1^{+1.3}_{-0.9}$. This rate is more than a factor of 2 larger than the rate measured for $^{12}_{\Lambda}$C in the present work. It seems unlikely that the lifetime would change so dramatically with such a small change in mass, but a detailed calculation is needed.

The quantities Γ_n/Γ_p and $\Gamma_{\text{nm}}/\Gamma_{\pi^-}$ have been previously measured in the mass region $10\leq A\leq12$ by Montwill *et al.*[13] (see Table II). This experiment produced hypernuclei by the absorption of stopped K^-'s in an emulsion stack and the production of a hypernucleus was determined by the detection of an energetic π^-. Their results for the ratio Γ_n/Γ_p agree with the present results at the extreme of the errors, while their values for

TABLE VI. $^{12}_{\Lambda}$C experimental results.

$^{12}_{\Lambda}$C state	Decay hypernucleus	$\Gamma_{\text{total}}/\Lambda_{\Lambda}$	$\Gamma_{\text{nm}}/\Gamma_{\Lambda}$	Γ_n/Γ_p	$\Gamma_{\pi^-}/\Gamma_{\text{nm}}$
g.s.	$^{12}_{\Lambda}$C	1.25 ± 0.18	1.14 ± 0.20	$1.33^{+1.12}_{-0.81}$	<0.14 (95% C.L.)
$p^{-1}p$	$^{11}_{\Lambda}$B	1.37 ± 0.16		$1.04^{+0.59}_{-0.48}$	
$s^{-1}s$	unknown	1.31 ± 0.20			

the ratio $\Gamma_{nm}/\Gamma_{\pi^-}$ disagree with the present measurements by a factor of 2–4.

B. Comparison of the $^{12}_{\Lambda}$C and $^{5}_{\Lambda}$He experimental results

A comparison of Tables V and VI shows that there are significant changes in the decay mechanisms of $^{12}_{\Lambda}$C and $^{5}_{\Lambda}$He. These can be largely attributed to the changing number of nucleons available for nonmesonic decay and to the changing effectiveness of Pauli blocking in suppressing the mesonic decay modes.

The total nonmesonic decay rate Γ_{nm} drops by a factor of 2.6 in going from $^{12}_{\Lambda}$C to $^{5}_{\Lambda}$He, scaling with the number of nucleons available for nonmesonic interactions. The $^{209}_{\Lambda}$Bi and $^{238}_{\Lambda}$U lifetime data[31,32] indicate, however, that this scaling appears to saturate for large-A nuclei. Furthermore, a dramatic mass dependence is seen in the $\Gamma_{nm}/\Gamma_{\pi^-}$ ratio, which drops by a factor of 20 in going from $^{12}_{\Lambda}$C to $^{5}_{\Lambda}$He. This increase in mesonic decay rate could be partly due to the reduced binding energy and partly due to the open P shell in $^{5}_{\Lambda}$He. The latter could also change the nonmesonic decay. The nuclear structure differs between $^{12}_{\Lambda}$C and $^{5}_{\Lambda}$He since we expect a much larger probability for P-wave Λ-N initial states in $^{12}_{\Lambda}$C than in $^{5}_{\Lambda}$He.

C. Comparison of the experimental results to calculations

The Hamiltonians used in the calculations of the nonmesonic decay rates include the meson-exchange and quark-quark Hamiltonians listed in Eqs. (1) and (3). For $^{5}_{\Lambda}$He, meson-exchange calculations have been performed by Dubach, Donoghue, Holstein, de La Torre, and Kimura,[44] Takeuchi, Takaki, and Bando,[45] and Oset and Salcedo.[46]

Dubach *et al.* find $\Gamma_{nm}=0.5\Gamma_{\Lambda}$ by using the exchange of π, ρ, η, ω, K, K^* mesons to describe the nonmesonic transition. Takeuchi *et al.* find the range of values $\Gamma_{nm}/\Gamma_{\Lambda}=0.033\rightarrow0.450$, where the limits correspond to completely destructive and constructive interference between the π and ρ exchange contributions used in the calculation. Both these calculations are able to show consistency with the experimental value for Γ_{nm}. The Oset and Salcedo calculation accounts for the effect of pion propagation through the nuclear medium. They find $\Gamma_{nm}=1.1\Gamma_{\Lambda}$ for $^{5}_{\Lambda}$He. The Dubach calculation finds $\Gamma_n/\Gamma_p=0.48$ for $^{5}_{\Lambda}$He, while Takeuchi *et al.* report a very small value, $\Gamma_n/\Gamma_p=0.02$, when they choose a phase between the contributions of π and ρ exchanges which best describes Γ_{nm}. The other authors do not report a value for Γ_n/Γ_p.

Several calculations have been reported which predict the value of the nonmesonic decay rates of $^{12}_{\Lambda}$C, which include meson-exchange calculations by Oset and Salcedo[46] (π exchange only) and Dubach *et al.*[44] (π, ρ, η, ω, K, K^* exchange). Oset and Salcedo find $\Gamma_{nm}=1.4\Gamma_{\Lambda}$, and Dubach *et al.* find $\Gamma_{nm}=1.2\Gamma_{\Lambda}$ for $^{12}_{\Lambda}$C, both of which are consistent with experiment. A composite approach has been developed by Heddle, Kisslinger, and Cheung,[47] in which a one-pion-exchange description of the weak interaction is used for ΛN separations greater than 1.0 fm, while at smaller separations the two baryons are treated as a six-quark state with quark-quark weak interactions given by the effective Hamiltonians of Gilman and Wise.[3] In this hybrid quark-hadron model, Heddle *et al.* find $\Gamma_{nm}=2.25\Gamma_{\Lambda}$ for the Gilman and Wise choice of Wilson coefficients. This corresponds to a $\Delta I=\frac{1}{2}$ enhancement factor of about 3.6 over $\Delta I=\frac{3}{2}$. Heddle and Kisslinger also point out that a phenomenological choice of the coefficients which gives a factor of 20 enhancement of $\Delta I=\frac{1}{2}$ will give $\Gamma_{nm}(^{12}_{\Lambda}\mathrm{C})=1.28\Gamma_{\Lambda}$, in agreement with this experiment.

A meson-exchange calculation has been performed for nuclear matter by McKellar and Gibson[48] (π and ρ exchange), where they find the value $\Gamma_{nm}/\Gamma_{\Lambda}=1^{+1.0}_{-0.5}$. The McKellar and Gibson calculations are an expanded and corrected version of the earlier one-pion-exchange calculations of Adams.[49]

All of the $^{12}_{\Lambda}$C calculations obtain agreement with the experimental value of $\Gamma_{nm}/\Gamma_{\Lambda}=1.14\pm0.20$. Thus, calculations of more detailed quantities, in particular Γ_n/Γ_p, are very important to differentiate between the models. Only Dubach *et al.* report a preliminary value for Γ_n/Γ_p; their calculation of $\Gamma_n/\Gamma_p=0.83$ is in agreement with the experimental value of $1.33^{+1.12}_{-0.81}$. Any nonmesonic decay rate calculation whose largest term is one-pion exchange will tend to predict a Γ_n rate smaller than the measured value. In these calculations the $^3S\rightarrow{}^3D$ transition dominates due to the tensor character of the pion exchange and this leads to a small predicted value for the Γ_n partial rate since the ^3D final state is not allowed for two neutrons by exchange symmetry considerations. The Γ_n rate can be enhanced by including the contributions of heavier meson exchanges, as shown by Dubach *et al.* This calculation also shows the Γ_n rate may also be enhanced by (hyper)nuclear structure effects, for example, initial Λ-N P-wave states.

A number of calculations of mesonic rates have also been performed. Dalitz[50] has calculated the mesonic decay rates for $^{5}_{\Lambda}$He, with a result of $\Gamma_{\pi^-}(^{5}_{\Lambda}\mathrm{He})=0.22\Gamma_{\Lambda}$. This is somewhat less than the experimental value of

$$\Gamma_{\pi^-}(^{5}_{\Lambda}\mathrm{He})/\Gamma_{\Lambda}=0.43\pm0.10\ .$$

Oset and Salcedo[46] have calculated the total mesonic decay rate in $^{5}_{\Lambda}$He, and they find

$$\Gamma_{\mathrm{mesonic}}(^{5}_{\Lambda}\mathrm{He})/\Gamma_{\Lambda}=0.6\ .$$

The Oset and Salcedo result can be compared to the measured value of

$$\Gamma_{\mathrm{mesonic}}(^{5}_{\Lambda}\mathrm{He})/\Gamma_{\Lambda}=0.59^{+0.44}_{-0.31}\ .$$

Mesonic rate calculations have been performed for $^{12}_{\Lambda}$C by Motoba *et al.*[51] and by Oset and Salcedo.[46] Motoba *et al.* find

$$\Gamma_{\pi^-}(^{12}_{\Lambda}\mathrm{C})=0.066\Gamma_{\Lambda}$$

and

$$\Gamma_{\pi^0}(^{12}_{\Lambda}\mathrm{C})=0.96\Gamma_{\Lambda}\ .$$

They also calculate the mesonic decay of $^{11}_{\Lambda}$B, with the result that if the ground state of $^{11}_{\Lambda}$B is a $\frac{5}{2}^{+}$ state, the mesonic decay rates are

$$\Gamma_{\pi^-}(^{11}_{\Lambda}\mathrm{B})=0.158\Gamma_{\Lambda}$$

and

$$\Gamma_{\pi^0}(^{11}_{\Lambda}\mathrm{B})=0.080\Gamma_{\Lambda} .$$

Given that

$$\Gamma_{\mathrm{nm}}(^{12}_{\Lambda}\mathrm{C})/\Gamma_{\Lambda}=1.14\pm0.20$$

and that

$$\Gamma_{\mathrm{nm}}(^{12}_{\Lambda}\mathrm{C})/\Gamma_{\pi^-}=22^{+43}_{-12}$$

then

$$\Gamma_{\pi^-}(^{12}_{\Lambda}\mathrm{C},\mathrm{expt})/\Gamma_{\Lambda}=0.052^{+0.063}_{-0.035} ,$$

which is consistent with the Motoba calculation. Oset and Salcedo find

$$\Gamma_{\mathrm{mesonic}}(^{12}_{\Lambda}\mathrm{C})/\Gamma_{\Lambda}=0.4 ,$$

which can be compared to the experiment value of 0.11 ± 0.27.

V. CONCLUSIONS

The correct Hamiltonian for weak interactions in the presence of strong fields has been a topic of great interest in recent years. It is important for the analysis of meson and hyperon decays, plays a role in the analysis of *CP* violation, and presumably should explain the origin of the empirical $\Delta I=\frac{1}{2}$ rule.

Hypernuclei provide a convenient laboratory in which to study the baryon-baryon weak interaction and the associated effective weak Hamiltonian. The strangeness-changing process releases up to 176 MeV, providing a convenient signal for the decay of the strange quark. Of particular interest is Γ_{nm}, the nonmesonic decay rate for the process $\Lambda+N\rightarrow N+N$, which is not available for free-lambda decay. Our results for this quantity are in reasonable agreement with calculations which use an effective weak Hamiltonian derived from either meson exchange between baryons or W-boson exchange between quarks, as long as the isospin structure is adjusted so that the empirical $\Delta I=\frac{1}{2}$ rule is satisfied.

A second important parameter is the isospin-dependent quantity Γ_n/Γ_p which provides additional tests of these effective weak Hamiltonians. Although not yet well measured, initial results suggest a value significantly larger than many current calculations. Additional and more precise measurements of both these quantities in very light hypernuclei offer the opportunity to further specify the features of this Hamiltonians.

ACKNOWLEDGMENTS

We wish to acknowledge the assistance of D. Lazarus, Y. Makdisi, J. Mills, R. Meier, A. Esper, and the rest of the AGS staff. We also thank G. Wilkin of the Carnegie Mellon medium energy group for his considerable contributions to the experiment. This work was supported in part under Department of Energy (DOE) Grants DOE-FG02-87ER40315, DOE-FG05-88ER40419, and DOE-AC02-76CH00016.

*Present address: Department of Physics, Indiana University, Bloomington, IN 47405.
†Present address: University of Illinois Nuclear Physics Laboratory, 23 Stadium Drive, Champaign, IL 61820.
‡Present address: Mellon Institute, 4400 5th Avenue, Pittsburgh, PA 15213.
§Present address: Visidyne, Inc., 10 Corporate Place, South Bedford St., Berlington, MA 01803.
**Present address: Wheaton College, Wheaton, IL 60187.
††Present address: Institute for High Energy Physics, Beijing, China.
‡‡Present address: Brookhaven National Laboratory, Upton, NY 11973.
§§Present address: Department of Physics, Osaka University, Toyonaka Osaka, 560 Japan.

[1]N. Cabibbo, Phys. Rev. Lett. **10**, 531 (1963).
[2]D. Bailin, *Weak Interactions* (Sussex University Press, Sussex, 1977); E. D. Commins and P. H. Bucksbaum, *Weak Interactions of Leptons and Quarks,* (Cambridge University Press, Cambridge, 1983).
[3]F. J. Gilman and M. B. Wise, Phys. Rev. D **20**, 2392 (1979); Phys. Lett. **83B**, 83 (1979), and references therein.
[4]M. A. Shifman, A. I. Vainstein, and V. I. Zacharov, Nucl. Phys. **B120**, 316 (1977).
[5]C. B. Dover and G. E. Walker, Phys. Rep. **89**, 148 (1982); J. Cohen, Prog. Nucl. Part. Phys. **25**, 139 (1990).
[6]M. M. Block and R. H. Dalitz, Phys. Rev. Lett. **11**, 96 (1963); R. H. Dalitz, in Proceedings of the International Conference on Hyperfragments, St. Cergue, 1963, edited by D. Evans and W. O. Lock, European Organization for Nuclear Research (CERN) Report No. 64-1, 1964.
[7]R. Grace, P. D. Barnes, R. A. Eisenstein, G. B. Franklin, C. Maher, R. Reider, J. Seydoux, J. Szymanski, W. Wharton, S. Bart, R. E. Chrien, P. Pile, Y. Xu, R. Hackenburg, E. Hungerford, B. Bassalleck, M. Barlett, E. C. Milner, and R. L. Stearns, Phys. Rev. Lett. **55**, 1055 (1985).
[8]A. Sakaguchi, W. Bruckner, S. Paul, R. Schussler, and B. Povh, Nuovo Cimento A **102**, 511 (1989).
[9]M. M. Block, R. Gessaroli, J. Kopelman, S. Ratti, M. Schneeberger, L. Grimellini, T. Kikuchi, L. Lendinara, L. Monari, W. Becker, and E. Harth, Proceedings of the International Conference on Hyperfragments, St. Cergue, 1963, edited by D. Evans and W. O. Lock, European Organization for Nuclear Research (CERN) Report No. 64-1, 1964.
[10]N. K. Rao and M. S. Swami, Proc. Indian Acad. Sci. **71A**, 100 (1970).
[11]H. G. Miller, M. W. Holland, J. P. Roalsvig, and R. G. Sorensen, Phys. Rev. **167**, 922 (1968).
[12]I. R. Kenyon, A. Z. M. Ismail, A. W. Key, S. Lokanathan, and Y. Prakash, Nuovo Cimento **30**, 1365 (1963).

[13]A. Montwill, P. Moriarty, D. H. Davis, T. Pniewski, T. Sobczak, O. Adamović, U. Krecker, G. Coremans-Bertrand, and J. Sacton, Nucl. Phys. **A234**, 413 (1974).
[14]L. K. Mangotra, B. R. Sangal, M. L. Sharma, S. C. Gupta, T. Singh, Y. Prakash, and S. P. Goel, Nuovo Cimento **13A**, 826 (1973).
[15]J. P. Lagnaux *et al.*, Nucl. Phys. **60**, 97 (1964).
[16]S. N. Ganguli and M. S. Swami, Proc. Indian Acad. Sci. **66A**, 77 (1967).
[17]J. Cuevas, J. Diaz, D. M. Harmsen, W. Just, E. Lohrmann, L. Schink, H. Spitzer, and M. W. Teucher, Nucl. Phys. **B1**, 411 (1967).
[18]J. McKenzie, in *Proceedings of the International Conference on Hypernuclear Physics,* edited by A. R. Bodmer and L. G. Lyman (Argonne National Laboratory, Argonne, Ill., 1969), p. 403.
[19]G. Coremans, J. Sacton, D. O'Sullivan, F. Esmael, D. H. Davis, M. A. Shaukat, T. Pniewski, and J. E. Allen, Nucl. Phys. **B16**, 209 (1970).
[20]K. N. Chaudhari, S. N. Ganguli, N. K. Rao, M. S. Swami, A. Gurtu, and M. B. Singh, Proc. Indian Acad. Sci. **69A**, 78 (1969),
[21]N. W. Holland, Nuovo Cimento **32**, 48 (1964).
[22]R. J. Prem and P. H. Steinberg, Phys. Rev. **136**, 1803 (1964).
[23]G. Keyes, M. Derrick, T. Fields, L. G. Hyman J. G. Fekovich, J. McKenzie, B. Rieley, and I.-T. Want, Phys. Rev. D **1**, 66 (1970).
[24]G. Keyes, J. Sacton, J. H. Wickens, and M. M. Block, Nucl. Phys. **B67**, 269 (1973).
[25]G. Bohm *et al.*, Nucl. Phys. **B16**, 46 (1970).
[26]C. T. Murphy, in *Proceedings of the International Conference on Hypernuclear Physics,* edited by A. R. Bodmer and L. G. Hyman (Argonne National Laboratory, Argonne, Ill., 1969), p. 438.
[27]Y. W. Kang, N. Kwak, J. Schneps, and P. A. Smith, Phys. Rev. **139**, B401 (1965).
[28]R. E. Philips and J. Schneps, Phys. Rev. **180**, 1307 (1969).
[29]G. Bohm, J. Klabuhn, U. Krecker, F. Wysotzki, G. Bertrand-Coremans, J. Sacton, J. Wickens, D. H. Davis, J. E. Allen, and K. Garbowska-Pniewska, Nucl. Phys. **B23**, 93 (1970).
[30]K. J. Nield, T. Bowen, G. D. Cable, D. A. DeLise, E. W. Jenkins, R. M. Kalbach, R. C. Noggle, and A. E. Pifer, Phys. Rev. C **13**, 1263 (1976).
[31]J. P. Bocquet, M. Epherre-Rey-Campagnolle, G. Ericsson, T. Johansson, J. Konijn, T. Krogulski, M. Maurel, E. Monnand, J. Mougey, H. Nifenecker, P. Perrin, S. Polikanov, C. Ristori, and G. Tibell, Phys. Lett. B **182**, 146 (1986).
[32]J. P. Bocquet, M. Epherre-Rey-Campagnolle, G. Ericsson, T. Johnansson, J. Konijn, T. Krogulski, M. Maurel, E. Monnand, J. Mougey, H. Nifenecker, P. Perrin, S. Polikanov, C. Ristori, and G. Tibell, Phys. Lett. B **192**, 312 (1987).
[33]V. I. Noga, Yu. N. Ranyuk, N. Ya. Rutkevich, P. V. Sorokin, and E. V. Sheptulenko, Yad. Fiz. **43**, 1332 (1986).
[34]P. Pile, Proceedings of the the Third LAMPF II Workshop, Los Alamos Report No. LA-9933-C, 1983.
[35]R. A. Cecil, B. D. Anderson, and R. Madey, Nucl. Instrum. Methods **85**, 67 (1981).
[36]R. Bertini, O. Bing, P. Birien, K. Braune, W. Bruckner, A. Chaumeaux, M. A. Faessler, R. W. Frey, D. Garreta, T. J. Ketel, K. Kilian, B. Mayer, J. Niewisch, B. Pietrzyk, B. Povh, H. G. Ritter, and M. Uhrmacher, Nucl. Phys. **A368**, 365 (1981).
[37]L. Majling, M. Sotona, J. Zofka, V. N. Fetisov, and R. A. Eramzhyan, Phys. Lett. **92B**, 256 (1980).
[38]N. Auerbach and N. Van Giai, Phys. Lett. **90B**, 354 (1980).
[39]T. Cantwell *et al.*, Nucl. Phys. **A236**, 445 (1974).
[40]H. Bando, T. Yamada, and J. Zofka, Phys. Rev. C **36**, 1640 (1987).
[41]H. C. Chiang and J. Hufner, Nucl. Phys. **A352**, 442 (1981).
[42]A. Gal, private communication.
[43]H. Bando and H. Takaki, Prog. Theor. Phys. **72**, 106 (1984); Phys. Lett. **150B**,409 (1985); T. Motoba, K. Itonga, and H. Bnado, Nucl. Phys. **B489**, 683 (1988).
[44]J. Dubach, Nucl. Phys. **A450**, 71c (1986); *Intersections Between Particle and Nuclear Physics* (May 26–31, 1986, Lake Louise, Canada), Proceedings of the Second Conference on the Intersections of Particle and Nuclear Physics, AIP Conf. Proc. No. 150, edited by Donald F. Geesman (AIP, New York, 1986).
[45]K. Takeuchi, H. Takaki, and H. Bando, Prog. Theor. Phys. **73**, 841 (1985).
[46]E. Oset and L. L. Salcedo, Nucl. Phys. **A443**, 704 (1985).
[47]C.-Y. Cheung, D. P. Heddle, and L. S. Kisslinger, Phys. Rev. C **27**, 1277 (1983); D. P. Heddle and L. S. Kisslinger, *ibid.* **33**, 608 (1985); L. S. Kisslinger, in *Intersections Between Particles and Nuclear Physics* (May 26–31, 1986, Lake Louise, Canada), Second Conference on the Intersections of Particle and Nuclear Physics, AIP Conf. Proc. No. 150, edited by Donald F. Gessman (AIP. New York, 1986).
[48]B. H. J. McKeller and B. F. Gibson, Phys. Rev. C **30**, 322 (1984).
[49]J. B. Adams, Phys. Rev. **156**, 1611 (1967).
[50]R. H. Dalitz, in *Hypernuclear Physics,* Proceedings of the International School of Physics, "Enrico Fermi," Course 38, Varenna, 1966 (Academic, New York, 1967), p. 89.
[51]T. Motoba, K. Itonaga, and H. Bando, in *Proceedings of the 1986 INS International Symposium on Hypernuclear Physics,* edited by H. Bando, O. Hashimoto, and K. Ogawa (Organizing Committee of the 1986 INS International Symposium, Tokyo, 1986), p. 160.